Study of the Biomechanical Properties and Microstructure of Trabecular Musculi Pectinati in the Left Atrial Appendage for patients with Atrial Fibrillation

Shuaishuai Zhao[1,a], Zidun Wang[2], Qiang Chen[1], Liang Wang[1], Zhiyong Li [1,3*]

[1]School of Biological Science and Medical Engineering, Southeast University, Nanjing 210096, PR China
[2]First Affiliated Hospital, Nanjing Medical University, Nanjing, China
[3]School of Mechanical, Medical and Process Engineering, Queensland University of Technology (QUT), Brisbane, QLD, Australia

Abstract: Aims: (1) Quantitatively characterize the Pseudo Fibrosis Burden (PFB) of Left Atrial Appendage (LAA) Trabecular Musculi Pectinati (TMP) in patients with atrial fibrillation based on histological analysis; (2) Explore the passive dynamic properties of LAA TMP based on uniaxial tensile experiments and determine the hyperelastic constitutive parameters; (3) Explore samples Effects of different storage conditions on the mechanical properties of left atrial appendage TMP. Methods: Fifty TMP were isolated from the resected LAAs of 21 patients with atrial fibrillation and stored (23 strips in the -78°C cryopreservation group and 27 strips in the 4°C normal temperature storage group). The TMP stress-strain curve was obtained through uniaxial tension. According to this curve, the elastic modulus of the low strain zone (EMLS) and the high strain zone (EMHS) were respectively defined. The correlation between the TMP's diameter and its mechanical properties and the impact of storage temperature on TMP mechanics were analyzed. Four strain energy functions were used to fit the TMP stress-strain curve to obtain the hyperelastic model constitutive parameters. Histological analysis of the axial and transverse microstructure of TMP was performed using Verhoeff-Van Gieson double staining method of Elastic fibers and collagen fibers (EVG) and Masson staining respectively, and the Pseudo Fiber Burden (PFB) was calculated. Analyze the correlation between mechanical properties and PFB. Results: Cryopreservation reduced the elastic modulus in the hyperelastic stage of TMP mechanical properties. EMLS (r=-0.7228, P<0.0001)/EMHS (r=-0.6772, P<0.0001) showed a significantly negative correlation with TMP diameter, while PFB only showed a significantly higher positive correlation with EMHS (r=0.6646, P=0.0057). Conclusion: This study quantitatively characterized the morphological and mechanical features of TMP. The research revealed that different storage temperatures to some extent affected the mechanical properties of TMP. Moreover, there was a significant correlation between the mechanical properties of TMP and TMP diameter. This held potential significance for a deeper understanding of the mechanical aspects of TMP under atrial fibrillation conditions and for constructing atrial fibrillation simulation models of the LAA.

1. Introduction

The MP in the LAA is extremely important for the occurrence of thrombus in the LAA. From the perspective of the place where thrombus occurs, the location of atrial fibrillation thrombus mainly comes from the LAA. The proportion of valvular atrial fibrillation is 57%, while the proportion of non-valvular atrial fibrillation can be as high as more than 90% [1]. Furthermore, the site of thrombus generation is mainly in the area where TMP exist [2]. The existence of MP makes blood flow in the LAA prone to stasis. The extremely low wall shear strain rate of blood flow in the LAA is also concentrated near the MP [3]. More detailed studies have shown that the density [4] and distribution angle [5] of MP are closely related to the occurrence of thrombosis. From the perspective of the mechanical properties of the LAA, on the one hand, the active contraction of the LAA is also inseparable from the TMP. The existence of the LAA shares the blood pressure of the left atrium. More importantly, when the left atrium contracts actively, the LAA also contracts actively, and its contraction ability is stronger than that of the left atrium [6]. And the MP provide the active contractility of the LAA [7]. On the other hand, the LAA is in a non-contracting state more than 85% of the time [8]. Therefore, studying its passive mechanical properties has important clinical significance in determining its contractility and assessing the risk of thrombosis.

* Corresponding author: zylicam@gmail.com
[a]209750913@qq.com
Shuaishuai Zhao and Zidun Wang contributed equally to this paper.

As an indicator that cannot be ignored in patients with atrial fibrillation, the degree of fibrosis of the LAA has a high correlation with the development process of atrial fibrillation [9-10]. The fibrosis process of the LAA starts from the endocardium and myocardium, and finally Appearing in the epicardium [11], the endocardium of patients with atrial fibrillation will be thickened [12], and the main structures of TMP happen to be the endocardium and myocardium, which provides a component basis for the mechanical explanation of atrial fibrosis.

At present, experimental research on the in vitro passive mechanical properties of the human heart mainly focuses on the ventricular myocardium [13], heart valves [14] and left atrium [15], while there are fewer studies on the LAA. There is no lack of research on animal heart models. Among them, the most research on the atrial appendage is pig [16], sheep [17], etc. Although some animal models are often used to replace human samples in experimental mechanics to obtain tissue parameters, there are certain differences in morphology, biomechanics and histology between human and animal heart tissues. More importantly, the structure of the middle and end parts of the human LAA is extremely complex and irregular. In particular, the area not covered by the MP has a significantly different thickness than the area covered by the MP (Figure 1A). This is important when measuring the overall LAA. There are certain limitations in mechanical proper-ties. In order to more accurately measure the passive me-chanical properties of the LAA and the stability of the sample during mechanical testing, it is worth mentioning that the MP could be divided into adherent MP and TMP according to whether it is completely covered by the endo-cardium. The following studies would all focus on the TMP. (Figure 1B). The structure similar to this study is trabeculation from the ventricle [18], but there are no reports on the passive mechanical properties of human LAA TMP.

The in vitro mechanical testing of most biological tissue samples has differences in storage conditions [19-20], which will directly have a potential impact on the structure of biological tissue. The samples in this study were obtained as fresh as possible. It took no more than 3 hours from the time when the specimens was removed from the body to the completion of all tests.

2. MATERIALS AND METHODS

2.1. Materials and sample preparation

50 TMP (Figure 1B) with intact endocardium, uniform area, and completed mechanical testing were isolated from 21 patients (APPENDIX 1) with atrial fibrillation (from First Affiliated Hospital, Nanjing Medical University, Nanjing, China) who underwent LAA resection, 23 of which were cryogenically stored at -78°C and subjected to uniaxial tensile mechanical testing within 48 hours. 27 of which were stored at 4°C after isolation and the mechanical tests were completed within 3 hours. The length of the TMP were generally less than 1cm and varied. In order to ensure that the tensile strain rate was consistent during the test and that the tissue did not fall off during the deformation process, tissues at both ends were reserved for fixation when separating TMP. On the loading platform (Figure 1C), the middle regular area was marked with graphite powder.

2.2. Uniaxial tension

The isolated TMP were tested using the uniaxial tension on the Uniaxial Stretching Platform (Kyle, Tianjin, China). The loading state was shown in Figure 1C. The tissues at both ends of the trabecular were fixed on hooks on both sides, compared with the previous testing that clips, sandpaper [21] or glue [22] to fix tissues, which could effectively prevent the sample from falling off. The TMP was pre-servered to 0.0005N state as the initial reference state[18], and 10 times of pre-stretching with a maximum strain of 50% was performed before officially collecting data to ensure it could be fully stretched, the loading waveform was a triangular wave, and the strain rate was 5%/s. A CCD camera (sampling frequency 10Hz) was set up directly above the sample to record the displacement changes between the marked points of the sample and the diameter of three different positions of the uniform area of TMP in the initial state. The collection of stress data was using the sensor device that comes with the instrument (sampling frequency is 50Hz). The self-written MATLAB code was used to extract the coordinates of the tissue marker points, and the peak value was used to collect the stress data. The displacement and peak stress data were registered and calculated at all times to obtain the stress and strain information. In order to solve the problem of large noise in the displacement data caused by uncontrollable factors such as instability between adjacent frames of the camera and subtle changes in the intensity of the surrounding light field, the Savitzky–Golay filter was used to filter it. The stress-strain curve of the TMP was similar to that of tendon [23], which is also a hyperelastic biomaterial (Figure 1D). It contained de-curling of fiber materials, especially collagen fibers, under low strains, and a linear deformation zone under high strains. The stress-strain tangent line of tissue strain in the range of 0-10% was defined as EMLS, and the elastic modulus in the linear elastic stage of the high strain zone was defined as EMHS.

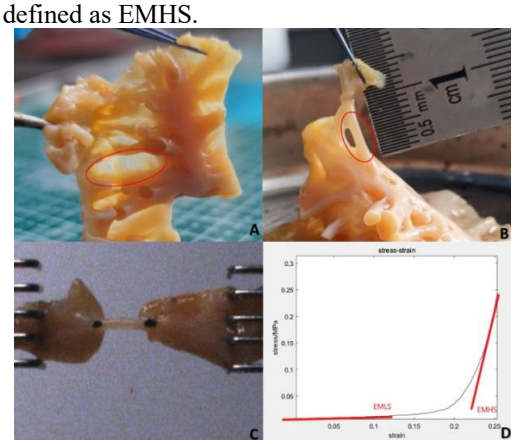

Figure 1. A: The thin area of LAA not covered by MP; B: The existence of TMP in LAA; C: Schematic of TMP fixation and loading; D: TMP true stress-strain curve.

2.3. Constitutive modeling

When the overall maximum strain of the material was 50%, the material didn't appear in the yield stage. Four different nonlinear isotropic hyperelastic material strain energy functions were used to fit the stress-strain relationship of TMP to the material stress-strain curve. Together, in the uniaxial tensile test, the Cauchy stress in the tensile direction are respectively

$$\sigma = C_1(2\lambda^2 - 2\lambda^{-1}) + C_2(2\lambda - 2\lambda^{-2}) + C_3(4\lambda^4 - 12\lambda^2 + 4\lambda + 12\lambda^{-1} - 8\lambda^{-2}) + C_4(6\lambda^3 - 6\lambda^2 - 6\lambda + 6\lambda^{-1} + 6\lambda^{-2} - 6\lambda^{-3}) + C_5(8\lambda^2 - 12\lambda - 4\lambda^{-1} + 12\lambda^{-2} - 4\lambda^{-4}) \quad (1)$$

$$\sigma = C_1\lambda^{C_2} - C_1\lambda^{-\frac{C_2}{2}} \quad (2)$$

$$\sigma = 2(\lambda^2 - \lambda^{-1})[C_1 + 2C_2(\lambda^2 + 2\lambda^{-1} - 3) + 3C_3(\lambda^2 + 2\lambda^{-1} - 3)^2] \quad (3)$$

$$\sigma = C_1\left(\lambda^2 - \lambda^{-1}\right)e^{C_2\left(\lambda^2 + 2\lambda^{-1} - 3\right)} \quad (4)$$

(1) is the Cauchy stress expression corresponding to the second-order Mooney-Rivlin strain energy function, (2) is the Cauchy stress expression corresponding to the first-order Ogden strain energy function, (3) is the Cauchy stress expression corresponding to the Yeoh strain energy function, (4) is the Cauchy stress expression corresponding to the Fung strain energy function.

where σ is the Cauchy stress in the tensile direction, λ is the main elongation, and C_i (i=1~5)is the material constant. When the strain of the sample was in the range of 0 to 10%, it was approximately in the linear elastic stage. When the strain exceeded 25%, some sample data did not exist. In order to unify the calculation, the data in the above stages were removed during data fitting, and only 10% to 25% Interval data were fitted, and the data fitting was based on Levenberg-Marquardt nonlinear regression algorithm, and the goodness of fit was determined by the R^2 value.

2.4. Microstructural analysis

For the samples stored in the frozen group, the dye solution could not fully combine with the tissue under long-term PBS infiltration, so all of the sources of the stained samples were from the fresh group. After testing, the fresh group samples were quickly transferred to 4% paraformaldehyde solution for fixation. After 24 hours, the regular areas of the samples were dehydrated, made transparent and embedded in paraffin, and carefully sectioned continuously along the transverse and axial directions of the regular areas of the TMP. 4μm thick and subsequently embedded in paraffin. The processed tissue sections were stained with Masson and EVG to mark the distribution of TMP collagen, elastin and muscle fibers respectively. Image J was used to determine the components of the transverse section, and a self-written MATLAB program was used to determine the composition of the transverse section. Endocardial thickness was measured. Referring to the formula for calculating the degree of myocardial fibrosis [24], the TMP cross-section PFB (5) was calculated using the percentage of blue collagen fibers in the entire cross-sectional area under Masson staining of transverse sections, and its correlation with the EMLS and EMHS of the sample was analyzed.

$$PFB = \frac{\text{fibrosis area[blue]}}{\text{fibrosis area[blue]} + \text{card muscle area[red]}} \times 100\% \quad (5)$$

2.5. Statistics

The Shapiro-Wilk test was selected for the normality test of the measurement results. The results that did not conform to the normal distribution were presented in the form of median + interquartile range, and the data that conformed to the normal distribution were presented in the form of mean ± standard deviation. Statistical data were processed in SPSS 26, and the drawing tool was GraphPad Prism 8.0.1. Non-parametric difference analysis used the Mann-Whitney U test, and $p<0.05$ was considered to be significantly different. The correlation between two non-normally distributed variables was analyzed using Sperman correlation, and $p<0.05$ was considered to have a significant correlation.

3. Results

3.1. Histology and mechanical properties of TMP within LAA

The structure in the LAA cavity was extremely complex, and the wall thickness was very uneven. The thickness of the wall surface not covered by the MP was less than 0.5mm [25], about 0.3964±0.0719mm, which was much smaller than other areas covered by the MP. In comparison, the structure of the TMP was relatively simple and could be approximately regarded as a cylinder. By comparing the cross-sectional area derived from the measurement of the macroscopic TMP diameter with the full area obtained by staining longitudinal tissue sections, the area deviation was (4.07±3.29) %. For the 50 TMP (APPENDIX 1) of isolated TMP, the diameter was 1.552 (1.217,2.264) mm, EMLS was 0.028 (0.014,0063) MPa, and EMHS was 5.586 (2.950,13.565) MPa. From a transverse cross-sectional, the composition of the TMP primarily included collagen, elastin, and muscle fibers. The structure was relatively regular, comprising predominantly collagen in the peripheral endocardium, with a small amount of punctate elastin distributed near the muscle fibers (constituting less than 10%). In some specimens, there was also a distribution of circular collagen structures within the muscle fibers. Examining the longitudinal structure, the small TMP muscles demonstrated a stable and uniform arrangement along the axis, with muscle fibers aligned axially. Elastin proteins were distributed on the side near the muscle fibers, exhibiting a certain degree of curvature (depicted in Figure2 E's black region). The endocardial thickness was measured at 124.55(95.885,158.06)μm, showing a positive correlation with the diameter of the small trabeculae(r=0.5670, P=0.0017). PFB exhibited a positive correlation with EMHS (r=0.6646, P=0.0057), while no significant correlation was observed between PFB and EMLS (r=0.2869, P=0.1643).

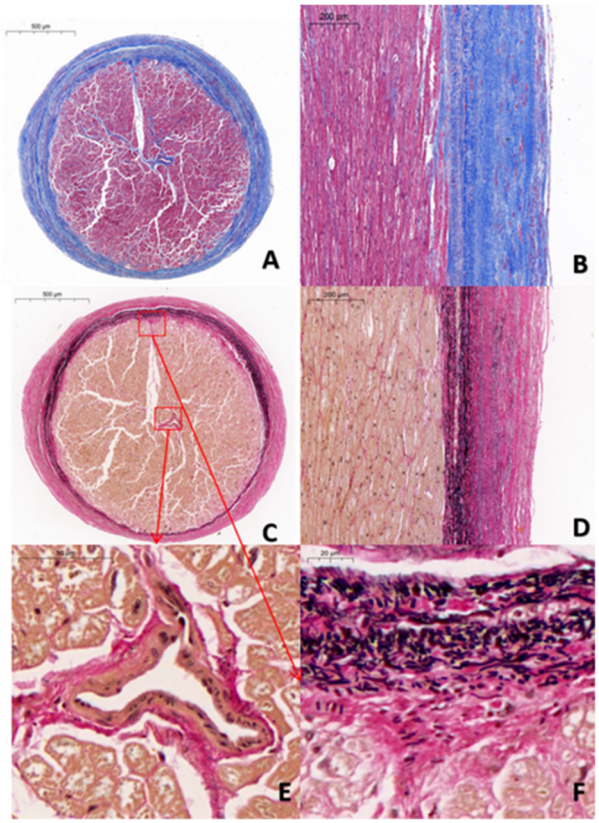

Figure 2. Microstructure of TMP. A: Circumferential cross-section (Masson); B: Longitudinal section of TMP(Masson); C: Circumferential cross-section (EVG); D: Longitudinal section of TMP(EVG); E: Speckled elastic fibers; F: Longitudinal section of TMP(EVG);

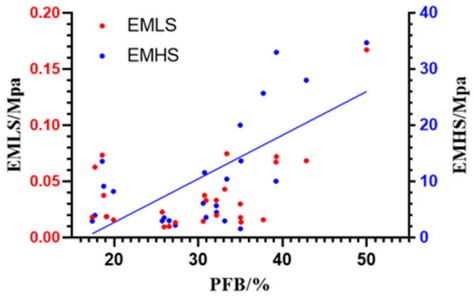

Figure 3. The relationship between PFB and EMLS&EMHS

3.2 Effects of different storage conditions on the mechanical properties of TMP

After comparing the two groups of TMP's EMLS and EMHS with different storage conditions, it was found that there was no significant difference between EMLS (P=0.893>0.05) and EMHS (P=0.499>0.05) under different storage conditions (Figure 4). Among them, FEMLS was 0.032 (0.010,0063) MPa, FEMHS was 5.495 (2.509, 15.520) MPa, NEMLS was 0.029 (0.020,0050) MPa, and NEMHS was 6.089 (2.970, 13.550) MPa. However, in the 10% to 25% hyperelastic section, the frozen group had a certain mechanical loss compared to the fresh group (Figure 5). No matter what the storage conditions were, EMLS and EMHS both decreased with the increase of TMP diameter (Table 1).

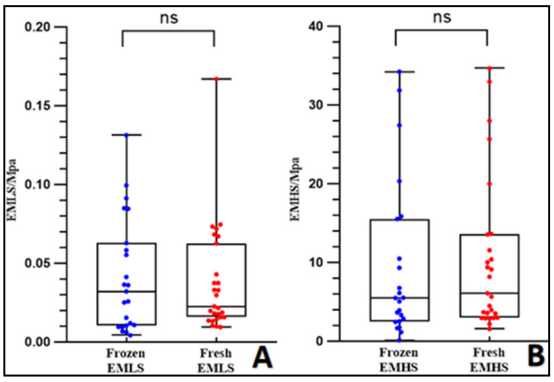

Figure 4 Boxplot. A: The impact of storage conditions on EMLS; B: The impact of storage conditions on EMHS.

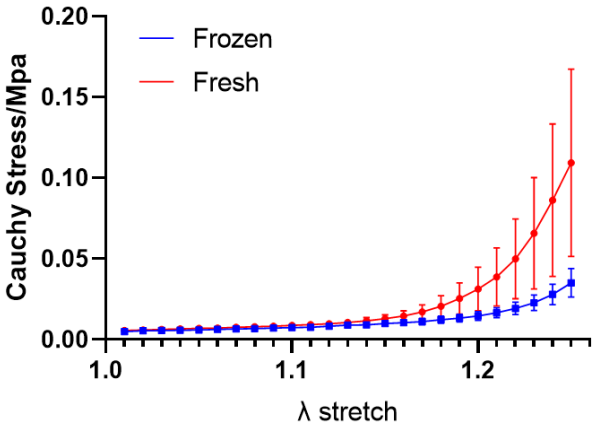

Figure 5 Uniaxial tension Cauchy stress- elongation(λ) curves of TMP under different storage conditions

Table 1. Correlation analysis between TMP diameter (D) and mechanical properties of TMP

	Spearman	*P*
D vs EMLS	-0.7228	<0.0001****
D vs EMHS	-0.6772	<0.0001****
D vs FEMLS	-0.8947	<0.0001****
D vs FEMHS	-0.7624	<0.0001****
D vs NEMLS	-0.417	0.031*
D vs NEMHS	-0.6594	0.0002***

Notes: F:Frozen; N:Normal(=Fresh)

3.3. Constitutive model

All four models were able to capture the mechanical behavior of the TMP MP well (APPENDIX 2) (R^2>0.9). The frozen group and fresh group both had the best fitting results for second-order Mooney-Rivlin, with goodness of fit of 0.9876 and 0.9981, respectively (APPENDIX 2).

4. Discussion

This study mainly characterized and quantified the mechanical properties and microstructure of TMP within the LAA. As an important sub-morphological parameter of LAA, the distribution of TMP had a strong correlation with the occurrence of cardioembolic strokes. Specifically,

the density of the MP demonstrated better universality in relation to stroke occurrence when compared with the classification based on LAA shape. From the perspective of passive testing, compared with the overall measurement of the passive mechanical properties of the LAA, from the perspective of the uniformity of the approximately regular circular and longitudinal structures of the transverse section, the TMP's structure was simpler (the overall structure is approximately cylindrical), and the test results were relatively more stable. Structurally speaking, the main components of the TMP cross section were muscle fibers and collagen fibers, which could perfectly correspond to the definition of tissue fibrosis, and thus could be soft tissue mechanical properties were linked to fibrosis. However, if elastic fiber was further included, there would be certain difficulties because of its low proportion.

The storage conditions didn't exert a significant influence on TMP's EMLS and EMHS. However, a noticeable decline in the mechanical properties of the hyperelastic segment tissue was observed when subjected to cryopreservation conditions ranging from about 10% to 25% strain. In comparison to cartilage [26], which are predominantly composed of non-cellular structures and can maintain their mechanical properties through repeated freezing and thawing, tissues with a substantial cellular component, such as liver [19] and arterial [27], experienced significant alterations. This underscores the fact that cryoinjury to cardiomyocytes under trabecular micro-scopic conditions indeed impacted their biomechanical properties at the macroscopic mechanical properties.

Four different isotropic hyperelastic materials were used to quantitatively characterize trabecular muscle structure. In the fresh tissue group, the fitting goodness of both second-order Mooney-Rivlin and Yeoh models exceeded 99%, providing a reference for extra-corporeal bio-mechanical simulations of the LAA. However, data from uniaxial tensile experiments alone couldn't fully characterize the passive response of TMP or even the entire LAA. While the structure within the trabecular was relatively uniform, it was not isotropic when viewed as a whole. Differences in components and the orientation of fibers could result in different mechanical responses. To comprehensively determine tissue properties, additional experimental strategies, such as biaxial tension and triaxial shear tests, need to be incorporated.

Both EMLS and EMHS exhibited a radius-dependent decrease. Considering the mechanical differences in various structural components within soft tissues, it was inferred that the decrease was attributed to the smaller increase in the thickness of the endocardium, mainly composed of collagen fibers, compared to the overall radius increase. This resulted in a gradual decrease in the proportion of collagen fibers. Using PFB to define the "fibrosis" degree of TMP, the results showed a significant positive correlation between the dominant stage of EMHS and PFB, suggesting that the decrease in EMHS was due to the decreasing proportion of collagen fibers with the increasing radius of the tissue. For patients with atrial fibrillation, there was a significant increase in the thickening of the endocardium [28], analogous to the tissue. This led to an increase in PFB, an increase in tissue elastic modulus, and a decrease in tissue compliance. In addition, according to the distribution of MP in LAA, MP close to the LAA orifice were relatively thick. As they moved away from the LAA orifice, MP continued to branch and become thinner like a tree trunk [29]. As a type of MP, the mechanical properties of TMP showed that MP exhibited a higher elastic modulus than the thicker MP closer to the LAA orifice, the compliance of the MP decreases with increasing distance from the LAA orifice.

Acknowledgments

The research was supported by the National Natural Science Foundation of China (12172089, 12372307, 61821002).

References

1. Beigel, R., Wunderlich, N. C., Ho, S. Y., Arsanjani, R., Siegel, R. J. (2014) The left atrial appendage: anatomy, function, and noninvasive evaluation. JACC Cardiovasc Imaging, 7: 1251–65.
2. Yamaji K., Fujimoto S., Yutani C., Hashimoto T., Nakamura S. (2002) Is the Site of Thrombus Formation in the Left Atrial Appendage Associated with the Risk of Cerebral Embolism? Cardiology., 97: 104–110.
3. Musotto, G., Monteleone, A., Vella, Danila D. L., Sofia V., Alessia P., Giuseppe Z., Bernardo P., Antonio C., Andrew B., Giorgia M., Burriesci, G. (2022) The Role of Patient-Specific Morphological Features of the Left Atrial Appendage on the Thromboembolic Risk Under Atrial Fibrillation. Front Cardiovasc Med., 9: 894187.
4. Khurram, I. M., Dewire, J., Mager, M., Maqbool, F. Zimmerman, S. L., Zipunnikov, V., Beinart, R., Marine, J. E., Spragg, D. D., Berger, R. D., Ashikaga, H., Nazarian, S., Calkins, H. (2013) Relationship between left atrial appendage morphology and stroke in patients with atrial fibrillation. Heart Rhythm., 10: 1843–9.
5. Liu, J., Yu, T., Tan, C., Li, H., Zheng, Y., Zheng, S. Wen, K., Wang, J., Geng, D., Zhou, S. (2023) How the trabeculae protrude within the left atrial appendage is the key factor affecting thrombosis in patients with atrial fibrillation. Int J Cardiovasc Imaging., 39: 2259-2267.
6. Pollick C., Taylor D. (1991) Assessment of left atrial appendage function by transesophageal echocardiography: Implications for the developme-nt of thrombus. Circulation., 84: 223-231.
7. Hondo, T., Okamoto, M., Yamane, T., Kawagoe, T., Karakawa, S., Yamagata, T., Matsuura, H. Kajiyama, G. (1995) The role of the left atrial appendage. A volume loading study in open-chest dogs. Jpn Heart J., 36: 225–34.
8. Hitch, D. C., Nolan, S. P. (1981) Descriptive analysis of instantaneous left atrial volume--with

special reference to left atrial function. J Surg Res., 30: 110–20.

9. Ma, N., Lu, R., Zhao, D., Jiang, Z., Tang, M., Bao, C., Mei, J.. (2020) Left Atrial Appendage Fibrosis and 3-Year Clinical Outcomes in Atrial Fibrillation After Endoscopic Ablation: A Histologic Analysis. Ann Thorac Surg., 109: 69–76.
10. Dzeshka, M. S., Lip, G. Y., Snezhitskiy, V., Shantsila, E. (2015) Cardiac Fibrosis in Patients With Atrial Fibrillation: Mechanisms and Clinical Implications. J. Am Coll Cardiol., 66: 943–59.
11. Grassinger, J. M., Henrich, M., Echevarria, A. C., Marz, I., Henrich, E., Bartel, A., Schneider, M., Aupperle-Lellbach, H. (2021) Correlation of Histopathological Changes in the Left Atrium and Left Atrial Appendage with the Degree of Dilation in Cats. J. Comp Pathol., 189: 8–25.
12. Shirani, J., Alaeddini, J. (2000) Structural remodeling of the left atrial appendage in patients with chronic non-valvular atrial fibrillation: Implications for thrombus formation, systemic embolism, and assessment by transesophageal echocardiography. Cardiovasc Pathol., 9: 95–101.
13. Nordsletten, D., Capilnasiu, A., Zhang, W., Wittgenstein, A., Hadjicharalambous, M., Sommer, G., Sinkus, R., Holzapfel, G. A. (2021) A viscoelastic model for human myocardium. Acta Biomater., 135: 441–457.
14. Vandemaele, P., Vander Linden, K., Deferm, S., Jashari, R., Rega, F., Bertrand, P., Vandervoort, P. Vander Sloten, J., Famaey, N., Fehervary, H. (2022) Alterations in Human Mitral Valve Mechanical Properties Secondary to Left Ventricular Remodeling: A Biaxial Mechanical Study. Front Cardiovasc Med, 9: 876006.
15. Bellini, C., Di Martino, E. S., Federico, S. (2013) Mechanical behaviour of the human atria. Ann Biomed Eng., 41: 1478–90.
16. Bellini, C., Di Martino, E. S. (2012) A mechanical characterization of the porcine atria at the healthy stage and after ventricular tachypacing. J Biomech Eng., 134: 021008.
17. Javani, S., Gordon, M., Azadani, A. N. (2016) Biomechanical Properties and Microstructure of Heart Chambers: A Paired Comparison Study in an Ovine Model. Ann Biomed Eng., 44: 3266–3283.
18. Fung, Y.C. (2013) Biomechanics: Mechanical Properties of Living Tissues. Springer Science & Business Media., San Diego.
19. Santago A.C., Kemper A.R., McNally C., Sparks J.L., Duma S.M. (2009) Freezing affects the mechanical properties of bovine liver. Biomedical Sciences Instrumentation., 45: 24–29.
20. O'Leary, S. A., Doyle, B. J., McGloughlin, T. M. (2014) The impact of long-term freezing on the mechanical properties of porcine aortic tissue. J. Mech Behav Biomed Mater., 37: 165–73.
21. Li, Z., Luo, T., Wang, S., Jia, H., Gong, Q., Liu, X. Sutcliffe, M. P., Zhu, H., Liu, Q., Chen, D., Xiong, J., Teng, Z. (2022) Mechanical and histological characteristics of aortic dissection tissues. Acta Biomater., 146: 284–294.
22. Bol, M., Iyer, R., Garces-Schroder, M., Kohn, S. Dietzel, A. (2020) Mechano-geometrical skeletal muscle fibre characterisation under cyclic and relaxation loading. J. Mech Behav Biomed Mater., 110: 104001.
23. Kubikova, T., Kochova, P., Brazdil, J., Spatenka, J. Burkert, J., Kralickova, M., Tonar, Z. (2017) The composition and biomechanical properties of human cryopreserved aortas, pulmonary trunks, and aortic and pulmonary cusps. Ann Anat., 212: 17–26.
24. Miyauchi, S., Tokuyama, T., Uotani, Y., Miyamoto, S., Ikeuchi, Y., Okamura, S., Okubo, Y., Katayama, K., Takasaki, T., Nakatani, N., Matsudaira, Y., Furusho, H., Miyauchi, M., Takahashi, S., Nakano, Y. (2022) Association between left atrial appendage fibrosis and thrombus formation: A histological approach. J Cardiovasc Electrophysiol., 33: 677–687.
25. Karim, N., Ho, S. Y., Nicol, E., Li, W., Zemrak, F. Markides, V., Reddy, V., Wong, T. (2020) The left atrial appendage in humans: structure, physiology, and pathogenesis. EUROPACE., 22: 5–18.
26. Mikheev, L. D. (2002) Photochemical lasers on electronic molecular transitions. Quantum Electronics., 32: 1122–1132.
27. Stemper, B. D., Yoganandan, N., Stineman, M. R. Gennarelli, T. A., Baisden, J. L., Pintar, F. A. (2007) Mechanics of fresh, refrigerated, and frozen arterial tissue. J Surg Res., 139: 236–42.
28. Shirani, J., Alaeddini, J. (2000) Structural remodeling of the left atrial appendage in patients with chronic non-valvular atrial fibrillation: Implications for thrombus formation, systemic embolism, and assessment by transesophageal echocardiography. Cardiovasc Pathol., 9: 95–101.
29. Hensey, M., O'Neill, L., Mahon, C., Keane, S., Fabre, A., Keane, D. (2018) A Review of the Anatomical and Histological Attributes of the Left Atrial Appendage with Descriptive Pathological Examination of Morphology and Histology. J. Atr Fibrillation., 10: 6–1650.

APPENDIX

APPENDIX 1. Correlation analysis between TMP diameter (D) and mechanical properties of TMP

Patient ID	Age	Sex (F/M)	Number of separated TMP	Number of completed tests	TMP ID	Diameter (mm)	EMLS (MPa)	EMHS (MPa)
3	65	M	3	1	0301	2.9335	0.01185	0.1189
5	64	M	3	2	0502	3.0910	0.05819	3.662
					0503	4.0235	0.01044	1.764
6	72	F	2	2	0601	3.1039	0.006796	2.509
					0602	3.9381	0.00621	1.151
9	59	F	2	2	0901	0.7010	0.09125	34.23
					0902	2.1359	0.009473	3.9
10	62	F	2	2	1001	1.6967	0.02505	5.037
					1002	2.9549	0.009643	3.322
12	64	F	2	2	1201	1.2374	0.08485	27.42
					1202	1.5582	0.03603	9.32
13	56	F	2	2	1301	1.9187	0.03208	2.462
					1302	2.2364	0.01544	6.109
16	52	M	2	2	1601	0.7047	0.09945	31.85
					1602	1.0234	0.0846	15.52
17	66	F	2	2	1701	1.8888	0.1313	5.495
					1702	2.9485	0.00421	1.634
20	53	F	2	1	2002	1.3694	0.0365	6.75
21	60	M	5	5	2101	1.1242	0.04126	20.31
					2102	2.0267	0.01069	5.512
					2103	1.2726	0.0628	15.86
					2104	2.2769	0.02575	2.84
					2105	1.2338	0.05525	10.48
22	75	M	2	2	2201	1.4700	0.04293	2.946
					2202	1.5028	0.03743	11.56
23	63	F	2	2	2301	0.9714	0.07318	13.55
					2302	1.5466	0.06253	3.959
24	60	F	4	4	2401	1.3538	0.01971	4.484
					2402	1.7708	0.03303	5.66
					2403	1.4045	0.01436	6.089
					2404	2.2601	0.009894	2.97
25	64	F	1	1	2501	2.1420	0.07198	32.96
27	71	F	1	1	2701	2.1420	0.01332	2.196
28	46	F	5	5	2801	0.9982	0.1669	34.64
					2802	1.4442	0.06714	10.03
					2803	2.4399	0.03284	3.579
					2804	1.1389	0.06825	27.97
					2805	2.6180	0.01783	1.547
29	77	M	3	2	2901	1.1088	0.07463	10.39
					2903	1.2437	0.01567	8.177
31	39	F	1	1	3101	1.4221	0.03749	9.109
32	65	M	5	5	3201	1.7648	0.02151	2.926
					3202	0.7950	0.02969	19.98
					3203	1.0316	0.01365	13.61
					3204	1.7146	0.009407	3.511
					3205	1.1660	0.01569	25.65
33	56	M	5	4	3301	2.4256	0.01875	3.696
					3303	1.5162	0.01045	9.375
					3304	2.7527	0.02258	2.951
					3305	1.8195	0.0181	2.91
Mean	61.38±9.13							

Notes: The missing patient number is a patient with unseparated effective TMP

APPENDIX 2. Correlation analysis between TMP diameter (D) and mechanical properties of TMP

	storage condition	C_1 (MPa)	C_2 (MPa)	C_3 (MPa)	C_4 (MPa)	C_5 (MPa)	R^2
Seccond Mooney-Rivlin	Frozen	-8.26±15.82	8.57±16.35	182.26±390.14	-442.82±941.60	276.08±581.90	0.9876
	Fresh	-5.67±9.90	5.89±10.26	116.55±210.66	-284.01±508.23	177.86±315.08	0.9981
Ogden	Frozen	0.14±0.34	16.30±16.08*	/	/	/	0.9027
	Fresh	0.42±0.76	11.77±13.12*	/	/	/	0.9144
Yeoh	Frozen	0.03±0.06	-0.39±1.08	2.39±6.35	/	/	0.9639
	Fresh	0.03±0.05	-0.29±0.74	1.69±5.00	/	/	0.9927
Fung	Frozen	0.02±0.02	10.56±10.99*	/	/	/	0.9505
	Fresh	0.02±0.01	7.51±8.07*	/	/	/	0.9664